Ensemble mean p_{t} versus charged-hadron multiplicities in high energy nuclear collisions

Thomas A. Trainor

Ensemble mean p$_t$ vs charged-hadron multiplicities in high energy nuclear collisions

Thomas A. Trainor

CENPA 354290, University of Washington, Seattle, WA 98195

Measurements of event-ensemble mean transverse momentum $\langle p_t \rangle$ vs charged-hadron multiplicity n_{ch} for p_t spectra from 5 TeV p-Pb and 2.76 TeV Pb-Pb collisions and from p-p collisions for several energies have been reported recently. While in all cases $\langle p_t \rangle$ increases monotonically with n_{ch} the rate of increase is very different from system to system. Comparisons with several theory Monte Carlos reveal substantial disagreements and lead to considerable uncertainty on how to interpret the $\langle p_t \rangle$ data. In the present study we develop a two-component (soft+hard) model (TCM) of p_t production in high energy nuclear collisions and apply it to the $\langle p_t \rangle$ data. The soft component is assumed to be a universal feature of high energy collisions independent of A-B system or energy. The hard-component model is based on the observation that dijet production in p-p collisions does not satisfy the eikonal approximation but does so in A-A collisions. Hard-component properties are determined from previous measurements of hadron spectrum hard components, jet spectra and fragmentation functions. The TCM describes the p-p and Pb-Pb $\langle p_t \rangle$ data accurately, within data uncertainties, and the p-Pb data appear to transition smoothly from p-p to A-A n_{ch} trends.

PACS numbers: 12.38.Qk, 13.87.Fh, 25.75.Ag, 25.75.Bh, 25.75.Ld, 25.75.Nq

I. INTRODUCTION

Proposed collision mechanisms that may determine hadron production in high energy nuclear collisions are strongly debated. Candidate mechanisms range from projectile nucleon dissociation and parton fragmentation to dijets [1–4] to color reconnection of multiple parton interactions [5], strong rescattering of partons and hadrons in a dense medium [6], hydrodynamic flows [7–9] or a colored-glass condensate [4, 10], possibly including glasma flux tubes [11]. Recent high energy data from the LHC and the emergence of apparently novel effects in p-A or d-A collisions have further stimulated debate.

It is safe to assume that there is a direct connection between underlying collision mechanisms and the structure of the hadronic final state in yields, spectra, correlations, and especially jets as hadron correlations. However, how to characterize the final-state structure statistically and how to interpret it in terms of physical mechanisms remains an open question. All analysis methods are susceptible to bias, the information in the data may not be fully exploited, and physical mechanisms are conventionally represented by Monte Carlo (MC) simulations based on complex assumptions that may be questioned.

In the present study we emphasize the first moment of the transverse momentum spectrum or event-ensemble mean p_t denoted by $\langle p_t \rangle$, its variation with collision system A-B, collision energy $\sqrt{s_{NN}}$ and charged-hadron multiplicity n_{ch}. Some previous studies include $\langle p_t \rangle$ vs n_{ch} measurements from p-p collisions at the Sp$\bar{p}$S [12] and RHIC [1], measurements of event-wise $\langle p_t \rangle$ fluctuations [13] and scale variation of those fluctuations in Au-Au collisions [14, 15], and variations of ensemble $\langle p_t \rangle$ with centrality in the Au-Au system [16]. Here we consider recent $\langle p_t \rangle$ vs n_{ch} data from the LHC for p-p, p-Pb and Pb-Pb collisions [17].

There are striking differences between $\langle p_t \rangle$ vs n_{ch} trends in p-p and A-A collisions. $\langle p_t \rangle$ tends to increase rapidly with n_{ch} in p-p collisions but much more slowly in A-A collisions. The p-A trend is intermediate. The trend of $\langle p_t \rangle$ increasing with centrality in A-A collisions is conventionally interpreted in terms of radial flow [18]. That interpretation suggests that the $\langle p_t \rangle$ trend in p-p collisions could also be associated with radial flow, with possibly larger magnitude. However, by the same argument if an alternative jet-related mechanism dominates $\langle p_t \rangle$ in p-p collisions that same mechanism could prevail in A-A collisions, misinterpreted there as radial flow [19].

We consider $\langle p_t \rangle$ vs n_{ch} data for several energies from 200 GeV to 7 TeV and from p-p or p-$\bar{p}$ collisions, Pb-Pb collisions and p-Pb collisions. We apply the two-component (soft+hard) model (TCM) of hadron production to $\langle p_t \rangle$ data systematics. We establish that jet production in p-p collisions has a simple dependence on the multiplicity soft component. We construct a TCM for $\langle p_t \rangle$ in p-p and A-A collisions and compare the TCM to data. We conclude that in all systems the increase in $\langle p_t \rangle$ with n_{ch} or A-A centrality is entirely due to jet production. Details of the $\langle p_t \rangle$ systematics in p-p collisions follow the properties of independently-measured jet spectra and dijet production. And $\langle p_t \rangle$ systematics in A-A collisions reflect previously-observed modification of jet structure in p_t spectra for more-central collisions. The p-Pb trend is simply explained as transitioning from p-p to A-A behavior as the number of nucleon participants in collisions becomes significantly greater than 2.

This article is arranged as follows: Sec. II introduces recent LHC $\langle p_t \rangle$ measurements with some conventional and alternative interpretations. Sec. III reviews the systematics of dijet production in 200 GeV p-p collisions. Sec. IV describes two-component models for $\langle p_t \rangle$ data from p-p and A-A collisions. Sec. V reviews $\langle p_t \rangle$ data from p-p collisions for several collision energies compared to the p-p TCM. Sec. VI reviews $\langle p_t \rangle$ data from 2.76 TeV Pb-Pb collisions compared to the A-A TCM. Sec. VII compares $\langle p_t \rangle$ data from 5 TeV p-Pb collisions with p-p

and Pb-Pb data and corresponding TCMs. Secs. VIII and IX present Discussion and Summary.

II. RECENT LHC $\langle p_t \rangle$ MEASUREMENTS

Reference [17] reports measurements of $\langle p_t \rangle$ vs n_{ch} for several collision systems at LHC energies, including p-p at 0.9, 2.76 and 7 TeV, p-Pb at 5 TeV and Pb-Pb at 2.76 TeV. Whereas $\langle p_t \rangle$ is calculated within a reduced p_t acceptance n_{ch} is extrapolated to $p_t = 0$. It is observed that $\langle p_t \rangle$ increases with n_{ch} much more rapidly for p-p collisions than for Pb-Pb collisions and that p-Pb data are intermediate, following the p-p trend for smaller n_{ch} and the form (but not magnitude) of the Pb-Pb trend for larger n_{ch}. Reference is made initially to similar previous measurements [1, 12] but no details are presented. It is anticipated that the $\langle p_t \rangle$ vs n_{ch} trends will shed light on underlying collision and hadron production mechanisms. In this section we review some conventional interpretations presented in Ref. [17] and possible alternatives relating to the TCM for high energy nuclear collisions.

A. Conventional interpretations

The $\langle p_t \rangle$ vs n_{ch} trend for 7 TeV p-p collisions is compared to the PYTHIA Monte Carlo [5]. Default PYTHIA 8 tune 4C (particular model-parameter selection) strongly disagrees with the p-p data and seems more compatible in form with the Pb-Pb results. However, when a so-called color reconnection (CR) mechanism is applied to multiple parton interactions (MPI) PYTHIA appears to describe the p-p data. The CR/MPI mechanism is referred to as a collective effect.

It is stipulated that any $\langle p_t \rangle$ increase with A-A centrality is conventionally attributed to radial flow of a dense medium, consistent with the so-called blast-wave model of A-A p_t spectra for which one model parameter is β_t, the radial flow velocity [9]. There should then be a direct relation between $\langle p_t \rangle$ and β_t through the A-A p_t spectrum. Some MC models of A-A collisions include radial and elliptic flow mechanisms [6, 8], but no theory model can describe the Pb-Pb $\langle p_t \rangle$ data of Ref. [17], all models deviating by tens of percent. In either p-p or Pb-Pb cases comparisons with linear-superposition models (of MPI or N-N collisions respectively) are said to fail. The large difference in $\langle p_t \rangle$ trends for given n_{ch} leads to questions about the role of n_{ch} in proposed collision mechanisms.

From comparisons among the three collision systems the argument is presented that since collectivity (flow) is assumed for A-A collisions in the form of a thermalized flowing dense medium, and some degree of collectivity may be present in p-p collisions via the CR/MPI mechanism, the intermediate behavior of the p-Pb data suggests that some form of collectivity may emerge there as well. Does radial flow play a role in p-Pb collisions, in p-p collisions? If $\langle p_t \rangle$ is a measure of radial flow is flow larger in p-p collisions? Other LHC results such as a claimed same-side "ridge" at large η in high-multiplicity p-p [21] and p-Pb [22] collisions suggest that flows may play a role at the LHC even in the smallest collision systems.

B. Alternative interpretations

Such deliberations omit a substantial amount of established information about jet production and manifestations thereof in the context of the two-component model of high energy nuclear collisions. Jet production is the signature manifestation of QCD in high energy collisions. Some aspects of jet production are predictable via perturbative QCD (pQCD), and some are accurately known via a broad range of measurements. Given the combination it is possible to make quantitative predictions for jet manifestations in hadron yields, spectra and correlations.

For instance, substantial jet fragment contributions to 200 GeV p-p [1] and Au-Au [16] collisions are described quantitatively by a combination of measured fragmentation functions [23] and minimum-bias (MB) jet spectra [3, 24]. The same hadron spectrum features attributed to radial flow [18] are fully consistent with QCD jets for all Au-Au centralities [19]. Certain jet-related structures in p-p and Au-Au angular correlations are also quantitatively related to single-particle spectrum structure by a QCD jet model [26–28].

The TCM provides an overarching framework for such comparisons. It assumes that the major contributions to yields, spectra and correlations consist of two components: (a) nucleon dissociation to soft hadrons and (b) scattered-parton fragmentation to correlated jets. Successful implementation of the TCM requires appropriate differential analysis methods and an accurate and comprehensive description of MB jet production. A TCM reference is defined as linear superposition of a fundamental process: small-x parton-parton interactions within p-p collisions or N-N interactions within A-A collisions. Deviations from a TCM reference may then reveal novelty in the composite system. The TCM has few parameters and a simple algebra, in contrast to most MC models. Below we apply the TCM to recent LHC $\langle p_t \rangle$ data.

III. DIJET PRODUCTION IN p-p COLLISIONS

To construct a TCM for $\langle p_t \rangle$ trends we must understand the systematics of dijet production in p-p collisions [1, 24–26]. The TCM includes soft and hard hadron production such that $n_{ch} = n_s + n_h$ within some angular acceptance $\Delta \eta$. It is assumed that n_s represents projectile nucleon dissociation and is proportional to the number of small-x partons released in the p-p collision. n_h then represents the number of hadron fragments from dijets and is proportional to the number of dijets in the acceptance. Within that context p-p p_t spectra can be

decomposed into fixed soft and hard components as described in Ref. [1] and briefly reviewed in App. A 1.

Figure 1 (left panel) shows y_t spectrum hard components $H(y_t, n_{ch})$ from ten multiplicity classes of 200 GeV non-single-diffractive (NSD) p-p collisions normalized by hard-component yield n_h within acceptance $\Delta\eta = 1$ [1]. Transverse rapidity for unidentified hadrons is defined as $y_t = \ln[(m_t + p_t)/m_\pi]$. The full y_t spectra are described accurately by the sum of two fixed model functions $S_0(y_t)$ and $H_0(y_t)$ (soft and hard model components) with relative amplitudes n_s (soft) and n_h (hard) [1]. Deviations of data $H(y_t, n_{ch})/n_h$ from model $H_0(y_t)$ below $y_t = 2.3$ ($p_t = 0.7$ GeV/c) for small n_{ch} values are significant and play a role in the $\langle p_t \rangle$ analysis below.
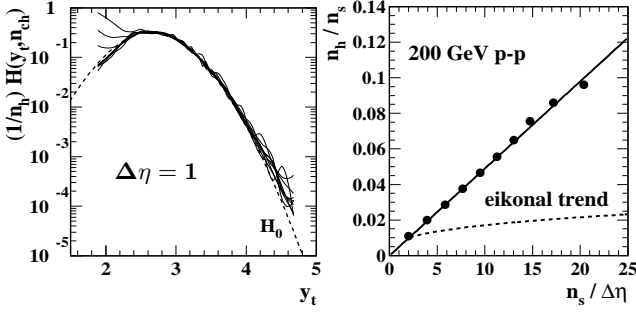

FIG. 1: Left: Hard components $H(y_t, n_{ch})$ for transverse-rapidity y_t spectra from eleven multiplicity classes of 200 GeV NSD p-p collisions normalized by hard multiplicity $n_h \approx \rho_h$ (within $\Delta\eta = 1$) [1]. The dashed curve is unit-normal hard-component Gaussian reference H_0. Right: The ratio of hard to soft multiplicity (solid dots) plotted vs the soft multiplicity density. The trend indicates that dijets scale as $n_h = \alpha n_s^2$ within $\Delta\eta = 1$ (solid line) inconsistent with the trend $n_s^{4/3}$ (dashed curve) implied by the eikonal approximation.

Figure 1 (right panel) shows the amplitudes of $H(y_t, n_{ch})/n_s$ vs soft multiplicity n_s. The line is $x = n_h/n_s = \alpha n_s$ consistent with $n_h = \alpha n_s^2$ for $\alpha \approx 0.006$ within acceptance $\Delta\eta = 1$. Substantial evidence supports the interpretation that n_s represents small-x fragments from projectile-proton dissociation, and n_h represents fragments from transverse-scattered-parton fragmentation [26, 29]. That interpretation is consistent with QCD calculations derived from measured FFs and measured dijet cross sections [3]. We then have a quantitative relation between hadron production via projectile dissociation and via scattered-parton fragmentation, with small-x partons (mainly gluons) as the common element.

If n_s is a proxy for participant small-x partons and MB dijet production scales accurately as n_s^2 we can conclude that the number of binary parton-parton collisions is $N_{bin} \propto N_{part}^2$, where $N_{part} \sim n_s$ represents the number of participant small-x partons in a p-p collision. The quadratic relation implies that any combination of participant partons can result in a large-angle dijet, *inconsistent with the eikonal approximation* where we expect $N_{bin} \propto N_{part}^{4/3}$ or equivalently $n_h/n_s \propto n_s^{1/3}$ as shown in Fig. 1 (right panel, dashed curve).

IV. TWO-COMPONENT MODEL FOR $\langle \mathbf{p_t} \rangle$

The TCM for yields, spectra and correlations is based on the assumption that hadron production near mid-rapidity proceeds via soft or hard mechanisms assumed to be linearly independent. The general TCM is further discussed in App. A. The soft component is assumed to be universal, the same for all systems and collision energies. The hard component follows a non-eikonal trend for p-p collisions and an eikonal trend for A-A collisions with larger A. The trend for p-A collisions is not known a priori but may involve a smooth transition from p-p to A-A. Within that context any increase in $\langle p_t \rangle$ with p-p n_{ch} or A-A centrality is attributed to increased jet production. Given those relations between hard and soft components we now define a TCM for $\langle p_t \rangle$ vs n_{ch}.

A. $\langle \mathbf{p_t} \rangle$ TCM for p-p collisions

To define ensemble $\langle p_t \rangle$ we begin with the concept of a total p_t denoted by P_t integrated within some angular acceptance. If n_{ch} is the total charge integrated within the same acceptance then $\langle p_t \rangle = P_t/n_{ch}$. Just as $n_{ch} = n_s + n_h$ we assume $P_t = P_{t,s} + P_{t,h}$. We then have $P_t = n_s \langle p_t \rangle_s + n_h \langle p_t \rangle_h$ and can define a TCM for p-p $\langle p_t \rangle$

$$
\begin{aligned}
\langle p_t \rangle_{pp}(n_s) &= \frac{n_s \langle p_t \rangle_s + n_h \langle p_t \rangle_h}{n_s + n_h} \\
&= \frac{\langle p_t \rangle_s + x(n_s)\langle p_t \rangle_h}{1 + x(n_s)},
\end{aligned} \tag{1}
$$

where $x(n_s) = \alpha n_s$ with α depending on the η acceptance. Given small adjustment of α for the experimental context we can derive n_s from n_{ch} by $n_s = (1/2\alpha)[\sqrt{1 + 4\alpha n_{ch}} - 1]$ since $n_{ch} = n_s + \alpha n_s^2$. The two $\langle p_t \rangle$ components can be inferred from the spectrum model functions $S_0(y_t)$ and $H_0(y_t)$ or from $\langle p_t \rangle$ vs n_{ch} data.

The above relation assumes that the entire p_t spectrum is integrated to obtain n_{ch} and P_t. If the spectrum is cut off at some small value $p_{t,cut}$ then for collision energy $\sqrt{s}$

$$
\begin{aligned}
\langle p_t \rangle'_{pp}(n_s, \sqrt{s}) &= \frac{n'_s \langle p_t \rangle'_s + n_h \langle p_t \rangle_h(\sqrt{s})}{n'_s + n_h} \\
&\approx \frac{\langle p_t \rangle_s + x(n_s)\langle p_t \rangle_h(\sqrt{s})}{n'_s/n_s + x(n_s)},
\end{aligned} \tag{2}
$$

where we assume no loss to the hard components of n_{ch} and P_t. As we demonstrate in the next section $n'_s \langle p_t \rangle'_s \approx n_s \langle p_t \rangle_s$. That is, $P_{t,s}$ is relatively insensitive to a p_t cutoff provided $p_{t,cut}$ is sufficiently small (typical for cases relevant to this study). In that case the only effect of the p_t cut is the ratio n'_s/n_s in the denominator. We also note explicit energy dependence as anticipated.

B. $\langle p_t \rangle$ TCM for A-A collisions

The TCM for A-A collisions is based on the Glauber model in which the fractional cross section (centrality) σ/σ_0 is related to geometry parameters N_{part} the number of projectile nucleon participants, N_{bin} the number of binary N-N encounters and $\nu = 2N_{part}/N_{bin}$ the mean participant pathlength in number of N-N encounters. The correspondence with observable n_{ch} can be established from the minimum-bias cross-section distribution on n_{ch}. For the present study the correspondence between Ref. [17] n_{ch} and Glauber model parameters was determined as described in Sec. VI.

For A-A collisions the TCM of Eq. (1) or (2) must be modified in three ways: (a) the multiplicity hard component increases with centrality as $n_h(\nu)$, (b) due to modified parton fragmentation to jets in more-central A-A collisions the spectrum hard-component shape changes (softens) with centrality leading to variation of $\langle p_t \rangle_h$ as $\langle p_t \rangle_h(\nu)$ and (c) an N-N "first encounter' effect must be accommodated, with details presented in Sec. VIII B.

The direct extension of p-p $n_{ch} = n_s + n_h$ to A-A is the first line of Eq. (3) where the N-N soft and hard components are scaled up by the corresponding Glauber parameters. However, the observed trend for hadron production in A-A collisions corresponds to n_h for the first N-N encounter being the same as that for p-p no matter what the A-A centrality. For $\nu - 1$ subsequent encounters n_h then transitions to a value depending on A-A centrality. The consequence is the second line that accurately describes n_{ch} trends for a variety of collision systems

$$n_{ch} = n_s(N_{part}/2) + \tilde{n}_h(\nu)N_{bin} \qquad (3)$$
$$\frac{2}{N_{part}}n_{ch} = n_{pp}[1 + x(\nu)(\nu - 1)].$$

In that line $n_{pp} = n_s + n_{h,pp}$ and $x(\nu) = n_h(\nu)/n_{pp}$. Note that $\tilde{n}_h(\nu)$ is an average over all ν N-N encounters whereas $n_h(\nu)$ or $x(\nu)$ applies only to the $\nu - 1$ subsequent encounters.

For a self-consistent description the same argument should be applied to $\langle p_t \rangle_h(\nu)$ such that in the first N-N encounter the p-p value holds while thereafter the value may change. The A-A TCM for $\langle p_t \rangle$ with p_t cut is then

$$\langle p_t \rangle'_{AA} = \frac{n_s\langle p_t \rangle_s(N_{part}/2) + \tilde{n}_h(\nu)\langle \tilde{p}_t \rangle_h(\nu)N_{bin}}{n'_s(N_{part}/2) + \tilde{n}_h(\nu)N_{bin}} \qquad (4)$$
$$= \frac{\langle p_t \rangle_s + x_{pp}\langle p_t \rangle_{h,pp} + x(\nu)\langle p_t \rangle_h(\nu)(\nu - 1)}{n'_s/n_s + x(\nu)(\nu - 1)}.$$

The Glauber model of A-A collisions based on the eikonal approximation gives the trend $N_{bin} \sim N_{part}^{4/3}$ or $\nu \sim N_{part}^{1/3}$ for participant nucleons. The equivalent for p-p collisions is inconsistent with the eikonal approximation, with $n_h \sim N_{bin} \sim N_{part}^2$ or $\nu \sim N_{part} \sim n_s$, where N_{part} in the latter case represents participant small-x partons. Equations (2) and (4) are employed below to analyze and interpret LHC $\langle p_t \rangle$ data from Ref. [17].

V. LHC p-p DATA

We first consider $\langle p_t \rangle$ vs n_{ch} measurements for p-p collisions at three energies. We review the effects of applied p_t cuts based on a simple spectrum soft-component model that enables direct comparisons with full-acceptance results. We then apply the TCM to $\langle p_t \rangle$ vs n_{ch} data and confirm that the eikonal model cannot be applied to p-p collisions. We then extract the collision-energy dependence of the $\langle p_t \rangle$ hard component. Comparison of that trend with the energy dependence of measured jet spectrum widths offers compelling evidence that $\langle p_t \rangle$ variation is a manifestation of jet production in p-p collisions.

A. Effects of p$_t$ acceptance cuts

The p-p spectrum hard component $H(y_t)$ is negligible below $p_t \approx 0.35$ GeV/c (Fig. 1, left panel). A p_t cut imposed below that point affects only the soft component. We can calculate the consequences with a soft-component model function. The unit-normal model function that describes spectrum soft components for both p-p and Au-Au collisions at 200 GeV is the Lévy distribution

$$S_0(y_t) = \frac{20.4}{[1 + (m_t - m_h)/nT]^n}, \qquad (5)$$

where m_h is the hadron mass (default is m_π), $T = 0.145$ GeV is the slope parameter and $n = 12.8$ is the Lévy exponent, with $m_t = m_h \cosh(y_t)$ and $p_t = m_h \sinh(y_t)$.

Figure 2 (left panel) shows unit-normal soft component $S_0(y_t)$ vs y_t (solid curve). Extrapolation to zero p_t is especially simple on transverse rapidity. For orientation y_t = 1, 2, 2.67, 3.35 and 4.05 correspond to p_t = 0.16, 0.5, 1, 2 and 4 GeV/c. The dashed curve shows $y_t S_0(y_t)$. The vertical hatched band indicates the nominal p_t acceptance cut for the Ref. [17] data. About 18% of the $y_t S_0(y_t)$ integral lies to the left of the band. However, the small-n_{ch} intercepts of $\langle p_t \rangle$ trends from Ref. [17] indicate that the effective p_t cut may be somewhat higher.

Figure 2 (right panel) shows the integral $\int_{p_{t,cut}}^{\infty} dp_t p_t S_0(p_t)$ (solid curve). The value is just the ratio n'_s/n_s of accepted to true soft-component multiplicities. The vertical hatched band marks the nominal acceptance cut for the analysis in Ref. [17]. The dashed curve shows the strong increase of $\langle p_t \rangle'_s$ with increasing p_t cut, whereas the dash-dotted curve shows the corresponding decrease in the total p_t soft component $P'_{t,s}$ (divided by the nominal NSD value of soft component n_s). The product $P_s = n_s \langle p_t \rangle_s$ is relatively insensitive to the p_t cut, and in what follows we assume that it does not change from the full-acceptance value.

B. p-p $\langle p_t \rangle$ data

Figure 3 (left panel) shows LHC $\langle p_t \rangle$ data from p-p collisions at 0.9, 2.76 and 7 TeV (upper points) [17]. The
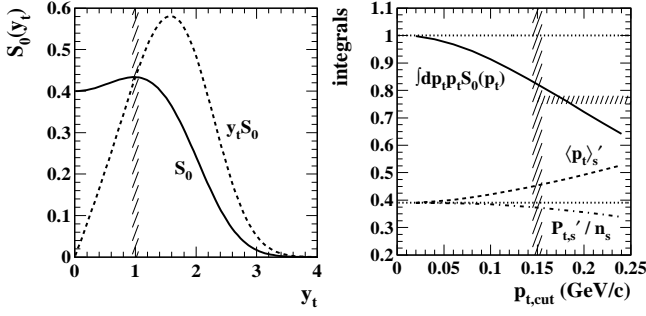
FIG. 2: Left: The p-p spectrum soft-component model $S_0(y_t) = (1/n_s)dn_s/y_t dy_t$ (solid curve) and product $y_t S_0(y_t)$ (dashed curve). The nominal p_t spectrum cutoff for Ref. [17] at 0.15 GeV/c is denoted by the hatched band. Right: The integral of $p_t S_0(p_t)$ above $p_{t,cut}$ vs the cut value (solid curve). The nominal cut position is denoted by the vertical hatched band. The horizontal hatched band indicates the range of n'_s/n_s ratios inferred from $\langle p_t \rangle$ data. The effect of the cut on $\langle p_t \rangle_s$ is denoted by $\langle p_t \rangle'_s$ (dashed curve). The dash-dotted curve labeled $P'_{t,s} = n'_s \langle p_t \rangle'_s$ indicates that the $P_{t,s}$ product is much less sensitive to the p_t cut for smaller cut values.

$\langle p_t \rangle'$ values were calculated with a nominal $p_{t,cut} = 0.15$ GeV/c. Charge multiplicity n_{ch} however was extrapolated to zero p_t. In Ref. [17] an apparent change of slope near $n_{ch}/\Delta\eta = 16$ is noted and compared to similar claims from other experiments. The curves are described below. Also included are lower-energy data from UA1 (open triangles, open circles [12]) and STAR (solid points [1]) for reference. The UA1 data for 900 GeV are high compared to the overall energy trend. The UA1 analysis inferred $\langle p_t \rangle$ values by fitting a "power-law" model function to p_t spectra. In Ref. [1] possible biases arising from that method are discussed. As demonstrated below, the curvature of the $\langle p_t \rangle$ vs n_{ch} trends arises because a jet contribution is common to both numerator and denominator of $\langle p_t \rangle$. The trends should saturate at the hard-component value $\langle p_t \rangle_h(\sqrt{s})$ for large n_{ch}.

Figure 3 (right panel) shows the quantity

$$\frac{n'_{ch}}{n_s}\langle p_t \rangle'(\sqrt{s}) - \langle p_t \rangle_s \approx x(n_s)\langle p_t \rangle_h(\sqrt{s}) \qquad (6)$$

where the expression on the right follows from Eq. (2), $\langle p_t \rangle_s = 0.385$ GeV/c is assumed for all cases and $x(n_s) = \alpha\, n_s/\Delta\eta$ with $\alpha = 0.0055$ for $\Delta\eta = 0.6$. The first term of $n'_{ch}/n_s = n'_s/n_s + n_h/n_s$ is determined such that the various data sets have a common intercept point. The ratio n'_s/n_s then has values within the horizontal hatched band in Fig. 2 (left panel) corresponding to $p_{t,cut} \approx 0.175$ GeV/c, slightly higher than the nominal cut value and suggesting some small uncorrected inefficiency near the acceptance boundary. Variation of the line slopes is discussed in the next subsection.
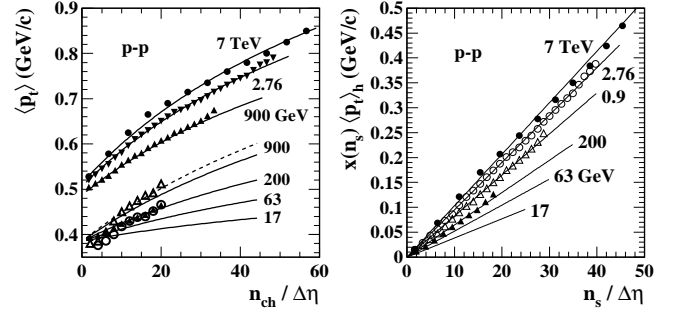
FIG. 3: Left: $\langle p_t \rangle$ vs n_{ch} for several collision energies. The upper group of points is from Ref. [17]. The lower 900 GeV data from UA1 derived from a "power-law" spectrum model [12] fall substantially above the TCM for that energy (solid curve) but are consistent with the TCM form with amplitude adjusted (dashed curve). Right: Data from the left panel multiplied by factor n'_{ch}/n_s that removes the jet contribution and the effect of the p_t cut on the soft component from the denominator of $\langle p_t \rangle$. The universal soft component $\langle p_t \rangle_s$ is then subtracted according to Eq. (6) isolating product $x(n_s)\langle p_t \rangle_h(\sqrt{s})$.

C. $\langle \mathbf{p_t} \rangle$ energy dependence and relation to MB jets

Figure 4 (left panel) shows the $\langle p_t \rangle$ data in the form

$$\frac{1}{x(n_s)}\left(\frac{n'_{ch}}{n_s}\langle p_t \rangle'(\sqrt{s}) - \langle p_t \rangle_s\right) = \langle p_t \rangle_h(\sqrt{s}) \qquad (7)$$

for four energies, where $\langle p_t \rangle_s$ has fixed value 0.385 GeV/c and $x(n_s)$ is defined above. Most of the $\langle p_t \rangle_h$ values fall in narrow horizontal bands, but the significant downturn for smaller multiplicities is a real change in the hard component for smaller n_{ch} first observed in p-p spectrum hard components at 200 GeV, for instance in Fig. 1 (left panel). The same effect apparently continues at least to 2.76 TeV. We find no evidence for a slope change in $\langle p_t \rangle$ vs n_{ch} near $n_{ch}/\Delta\eta = 16$ which would manifest in this figure as a significant step-wise decrease in $\langle p_t \rangle_h$ vs n_s.

Figure 4 (right panel) shows $\langle p_t \rangle_h(\sqrt{s})$ from the left panel (solid points) vs quantity $\Delta y_{max} = \ln(\sqrt{s}/3 \text{ GeV})$ from Ref. [24]. In that study it is shown that jet spectrum widths scale with p-p collision energy as Δy_{max}. Thus we conclude from the right panel of this figure that $\langle p_t \rangle_h$ is linearly related to the minimum-bias jet spectrum width. That trend is also consistent with the results of Ref. [3] where it is demonstrated that the spectrum hard component is predicted by folding an ensemble of fragmentation functions with a minimum-bias jet spectrum. In that case the hard-component width should scale linearly with the MB jet spectrum width, and $\langle p_t \rangle_h$ should have the linear correspondence to the jet spectrum width demonstrated above. For p-p collisions the $\langle p_t \rangle$ vs n_{ch} systematics compel a jet interpretation for the TCM hard component. The soft component remains consistent with a universal phenomenon independent of collision system or energy. The open symbols indicate predictions for lower energies. The hatched band represents the cutoff for dijet
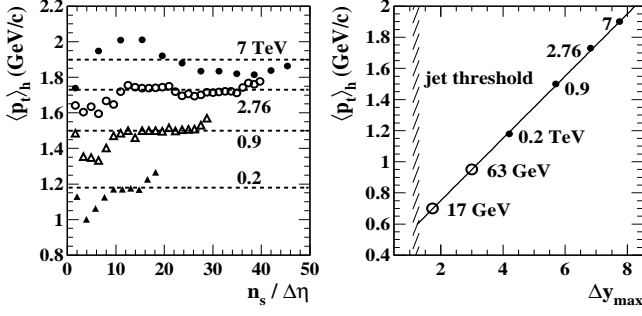
FIG. 4: Left: $\langle p_t \rangle$ hard components isolated according to Eq. (7). The data fall within narrow horizontal bands reflecting the point-to-point data consistency with the TCM. The decreases for smaller n_s reflect a real change in the hard component as seen in Fig. 1 (left panel) for 200 GeV spectra, here shown to be common to a range of collision energies. Right: The $\langle p_t \rangle_h$ mean values from the left panel plotted vs parameter $\Delta y_{max} = \ln(\sqrt{s}/3~\text{GeV})$ that describes variation of the minimum-bias jet spectrum width with p-p collision energy [24].
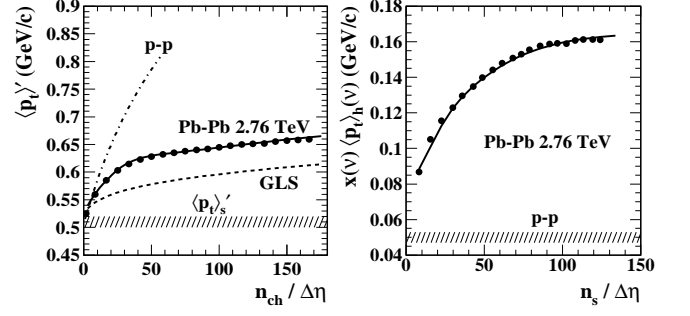
FIG. 5: Left: $\langle p_t \rangle'$ data for 2.76 TeV Pb-Pb collisions from Ref. [17] (points). The solid curve is the Pb-Pb TCM. The dashed curve is a Glauber linear superposition (GLS) reference assuming all N-N collisions are equivalent to p-p collisions and scale according to the Glauber model of Pb-Pb collisions following the eikonal approximation. $\langle p_t \rangle'_s = P_{t,s}/n'_{ch}$. Right: The product $x_h(\nu)\langle p_t \rangle_h(\nu) = P_{t,h}(\nu)/n_{pp}$ extracted from data in the left panel according to Eq. (8) with $x_{pp}\langle p_t \rangle_{h,pp} \approx 0.05$ GeV/c. The solid curve is part of the TCM.

production near $\sqrt{s} = 10$ GeV determined from angular correlation analysis [15, 27, 30].

VI. LHC Pb-Pb DATA

Figure 5 (left panel) shows 2.76 TeV Pb-Pb $\langle p_t \rangle$ data (points) from Ref. [17] as samples from the full data complement. As noted in that study $\langle p_t \rangle$ for Pb-Pb collisions increases much less quickly than that for p-p collisions (the 2.76 TeV p-p trend is the dash-dotted curve). It is also noted that the $\langle p_t \rangle$ increase in A-A collisions is conventionally attributed to radial flow corresponding to the blast-wave model applied to p_t spectra [18]. The hatched band shows the $\langle p_t \rangle$ soft component corresponding to $p_{t,cut} \approx 0.175$ GeV/c. The Glauber linear superposition (GLS) trend is Eq. (4) with $x = 0.028$ and $\langle p_t \rangle_h = 1.75$ GeV/c fixed at their 2.76 TeV p-p values. The solid curve through data is discussed below.

Figure 5 (right panel) shows the product $x(\nu)\langle p_t \rangle_h(\nu) = P_{t,h}(\nu)/n_{pp}$ (points) obtained from data in the left panel according to Eq. (4) by

$$x(\nu)\langle p_t \rangle_h(\nu) = \frac{\frac{2}{N_{part}}\frac{n'_{ch}}{n_s}\langle p_t \rangle' - \langle p_t \rangle_s - x_{pp}\langle p_t \rangle_{h,pp}}{\nu - 1} \quad (8)$$

The hatched band shows the NSD p-p value $x_{pp}\langle p_t \rangle_{h,pp} \approx 0.05$ GeV/c. The solid curve is discussed below. Those Pb-Pb results can be compared with Fig. 3 (right panel) for p-p collisions. We next isolate the individual factors.

Figure 6 (left panel) shows 2.76 TeV Pb-Pb hadron production data from Ref. [20] (points) compared to the corresponding TCM in the general form

$$\frac{2}{N_{part}}n_{ch} = n_{pp}[1 + x(\nu)(\nu - 1)] \quad (9)$$

where for 200 GeV Au-Au $n_{pp} \approx 2.5$, $x(\nu) \in [0.015, 0.095]$ and $x(1) = \alpha n_{s,NSD} = 0.015$. For 2.76 TeV the factor $1.85 \approx \ln(2760/10)/\ln(200/10)$ predicts the expected increase in $n_{s,NSD} \approx n_{pp} \to 4.6$ scaling with small-x partons as described in Ref. [24]. The same factor is applied to $x(\nu)$ per Sec. III . The functional form of $x(\nu)$ at 2.76 TeV is very similar to that at 200 GeV with the exception that the sharp transition (ST) in jet structure near $\nu = 3$ first reported in Ref. [27] has shifted down to $\nu \approx 2$ at the higher energy, as first noted in Ref. [31]. Eq. (9) with $x(\nu)$ defined below was used in this study to relate reported n_{ch} values from Ref. [17] to fractional cross sections and then to Glauber parameters $N_{part}/2$, N_{bin} and $\nu = 2N_{bin}/N_{part}$ according to the methods in Ref. [32].
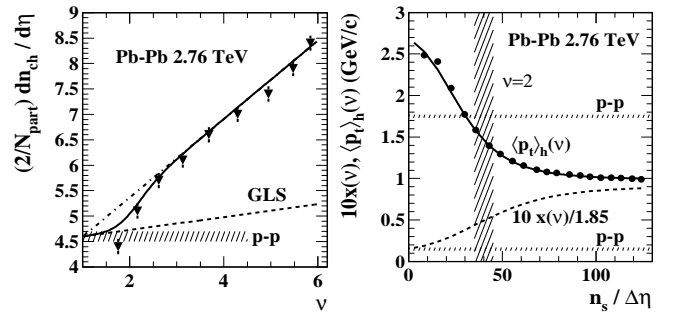

FIG. 6: Left: Hadron production data vs mean participant path length ν for 2.76 TeV Pb-Pb collisions from Ref. [20] (solid triangles). The lines and solid curve are the TCM for 200 GeV Au-Au collisions scaled up by factors 1.85 (soft component) and 1.85^2 (hard component) reflecting soft multiplicity n_s scaling as $\ln(\sqrt{s}/10~\text{GeV})$, as noted in Refs. [24, 31]. Right: The product data from Fig. 5 (right panel) divided by ratio model $x(\nu)$ defined by Eq. (10) and shown as the dashed curve in this panel. The solid curve is the $\langle p_t \rangle_h(\nu)$ model defined by Eq. (11). The combination is the basis for the Pb-Pb TCM.

Figure 6 (right panel) shows the $x(\nu)$ trend (dashed curve) that describes the ALICE hadron production data in the left panel (solid curve) defined by

$$x(\nu) = 0.028 + 0.141\{1 + \tanh[(\nu - \nu_0)/0.5]\}/2, \quad (10)$$

where $\nu_0 = 2$ estimates the ST for hadron production in 2.76 TeV Pb-Pb collisions. The 2.76 TeV $x(\nu)$ expression is divided by factor 1.85 in Fig. 6 for direct comparison with the 200 GeV trend. We can isolate factor $\langle p_t \rangle_h(\nu)$ by dividing the data in Fig. 5 (right panel) by $x(\nu)$ from Eq. (10). The result (solid points) is described by

$$\langle p_t \rangle_h(\nu) = 1.00 + 1.70\{1 - \tanh[(\nu - \nu_1)/0.42]\}/2 \quad (11)$$

with $\nu_1 = 1.75$ which defines the solid curve through data. Note that $\langle p_t \rangle_h(\nu)$ in Fig. 6 (right panel) describes an average over $\nu - 1$ secondary N-N encounters and for peripheral collisions does not extrapolate to the first-encounter p-p value 1.75 GeV/c. The product of Eqs. (10) and (11) gives the solid curve through data in Fig. 5 (right panel), and incorporated in Eq. (4) gives the solid curve through $\langle p_t \rangle$ data in the left panel of that figure.

The accurate TCM description of $\langle p_t \rangle$ data in Fig. 5 arises by construction from this analysis procedure. However, the procedure depends on several a priori elements: (a) the A-A $\langle p_t \rangle$ TCM represented by Eq. (4), (b) a TCM for hadron production represented by Eq. (9) that describes production at any collision energy modulo simple scaling with beam rapidity as discussed in Refs. [24, 31] and (c) p-p $\langle p_t \rangle$ trends accurately represented by a TCM whose energy dependence is consistent with universal jet spectrum properties as described in Ref. [24].

The new information is contained in Eqs. (10) and (11) which demonstrate a smooth $\tanh(\nu - \nu')$ transition from values in most-peripheral Pb-Pb (essentially N-N) collisions to modified constant values for more-central collisions. The transition in Pb-Pb is centered near $\nu = 2$ which corresponds to $N_{part}/2 \approx 9$ and $N_{bin} \approx 18$ with fractional cross section $\sigma/\sigma_0 \approx 0.68$. A similar transition is observed in 200 GeV Au-Au near $\nu = 3$ where $N_{part}/2 \approx 30$, $N_{bin} \approx 90$ and $\sigma/\sigma_0 \approx 0.5$. It may be more significant that at the two energies and corresponding path-length values the dijet density is approximately the same, $dn_j/d\eta \approx 2$ [31]. The hadron production trend at the two energies is related by a simple $\log(\sqrt{s_{NN}})$ energy scaling. The $\langle p_t \rangle_h \approx 1$ GeV/c value for more-central Pb-Pb at 2.76 TeV is the same fraction of the peripheral value (40%) as that at 200 GeV – 0.5 vs 1.2 GeV/c.

Figure 7 (left panel) shows the trends for $\langle p_t \rangle_h(\nu)$ and $x(\nu)$ on path length ν over a larger centrality interval. The trends for 2.76 TeV Pb-Pb collisions are the solid and dashed curves equivalent to Fig. 6 (right panel). The 2.76 TeV $x(\nu)$ trend is divided by 1.85 for direct comparison with the 200 GeV result. The dash-dotted curve shows $x(\nu)$ for 200 GeV Au-Au collisions with ST near $\nu = 3$ (fractional cross section $\sigma/\sigma_0 \approx 0.5$). There are no equivalent $\langle p_t \rangle_h(\nu)$ data for 200 GeV. We may conclude

from these $\langle p_t \rangle$ results that aside from translation of the ST from $\nu = 3$ to 2 jet modification in more-central A-A collisions at LHC energies is remarkably similar to that at RHIC energies.
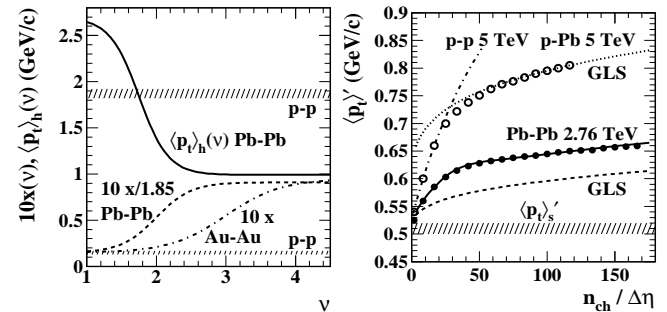

FIG. 7: Left: The model functions $x(\nu)$ (dashed curve) and $\langle p_t \rangle_h(\nu)$ (solid curve) plotted vs path length ν over a larger centrality interval ($\nu \approx 6$ for central A-A collisions). The $x(\nu)$ trend for 200 GeV Au-Au collisions (dash-dotted curve) is included for comparison. Corresponding 200 GeV $\langle p_t \rangle_h(\nu)$ data are not currently available. Right: $\langle p_t \rangle$ data for 5 TeV p-Pb collisions from Ref. [17] (open circles). The dash-dotted curve is the TCM for 5 TeV p-p collisions interpolated from the general p-p TCM developed in this study. The dotted curve is the GLS for Pb-Pb collisions (dashed curve) with ratio x increased by factor 2.5 and all else the same. The Pb-Pb data and TCM from Fig. 5 (left panel) are included for comparison.

VII. LHC p-Pb DATA

Figure 7 (right panel) shows p-Pb $\langle p_t \rangle$ data at 5 TeV [17] vs n_{ch} (open symbols). Also included for reference are the Pb-Pb results from Fig. 5 (left panel) and the TCM expression for the p-p trend at 5 TeV (dash-dotted curve). The upper GLS curve is the lower GLS curve assuming that constant x increases by factor 2.5 relative to NSD p-p but otherwise *jet structure is unchanged* in p-Pb collisions relative to p-p collisions: All p-Pb collisions are transparent. The GLS description of p-Pb data with A-A eikonal approximation for larger n_{ch} is good. The p-Pb data appear to make a smooth transition from the non-eikonal p-p trend to the eikonal A-A trend. The transition is located near $n_{ch}/\Delta\eta = 30$.

One can speculate that up to the p-Pb transition point there is only a single N-N collision in peripheral p-Pb and $\nu \equiv 1$. In that case the only way to satisfy the increasing n_{ch} condition is with increased N-N n_s resulting in a large increase in jet production $\propto n_s^2$ due to the non-eikonal interaction as in single p-p collisions. At some value of n_{ch} the probability for producing a single N-N collision with sufficient n_{ch} becomes smaller than the probability of a second N-N binary collision in more-central p-Pb collisions, and ν becomes significantly greater than 1. It is then possible to produce more soft hadrons relative to jets by multiple N-N collisions, each with a smaller soft

multiplicity n_s and therefore jets $\propto n_s^2$. It is interesting that the transition from non-eikonal to full eikonal behavior apparently occurs within a small n_{ch} interval.

VIII.   DISCUSSION

A.   Evolution of the HC in A-A collisions

Figure 7 (left panel) shows the trend of mean-p_t hard component (HC) $\langle p_t \rangle_h(\nu)$ vs 2.76 TeV Pb-Pb centrality including a transition from a larger peripheral value to a smaller central value, the ratio being about 2.5. The most rapid variation corresponds to a sharp increase in hadron production or sharp transition near $\nu = 2$. The same phenomenon is observed in hadron yields and spectra for Au-Au at 200 GeV, and a differential analysis of y_t spectra for identified hadrons including a two-component decomposition of the hadron spectra [16] reveals the spectrum hard-component centrality systematics which in turn determine $\langle p_t \rangle_h(\nu)$.

Figure 8 (left panel) shows the NSD p-p spectrum HC (points) from Ref [1]. The solid curve is a pQCD calculation of the p-p spectrum hard component based on (a) a parton (jet) spectrum with lower bound near 3 GeV integrating to 2.5 mb and (b) measured p-$\bar{p}$ fragmentation functions [3, 23]. The dash-dotted curve is the Gaussian approximation from Ref. [1]. The ensemble mean is $\langle p_t \rangle_h \approx 1.2$ GeV/c.
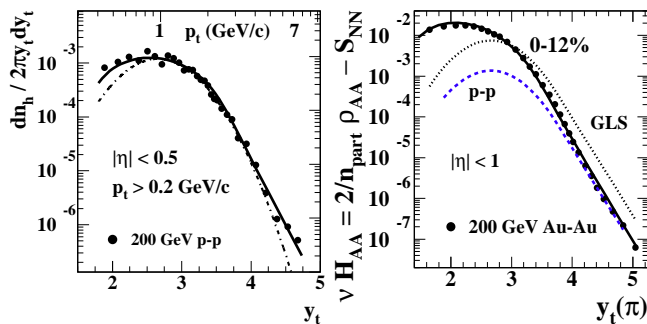

FIG. 8: Left: Spectrum hard component from 200 GeV NSD p-p collisions (points) [3]. The solid curve is a pQCD prediction for the corresponding fragment distribution derived from measured fragmentation functions and a dijet total cross section of 2.5 mb. Right: Spectrum hard component for 0-12% central 200 GeV Au-Au collisions (points) [16]. The solid curve is a pQCD prediction based on a simple modification of fragmentation functions [3]. The dotted curve is a GLS prediction of the TCM extrapolated from p-p collisions.

Figure 8 (right panel) shows the pion spectrum HC from 0-12% central 200 GeV Au-Au collisions (points) [16]. The dashed curve is the p-p Gaussian (with added power-law tail) from the left panel. The dotted curve is a GLS prediction for central Au-Au (assuming A-A transparency and ν increased by factor 5). The solid curve is a pQCD description of the central Au-Au data

based on a *single modification* of measured fragmentation functions (single parameter in a gluon splitting function) [3]. Fragment reduction at larger y_t is balanced by much larger fragment increase at smaller y_t conserving the parton energy *within resolved jets* [28]. The large increase in jet fragment production at smaller y_t is concealed by the biased conventional ratio measure R_{AA} [19]. The ensemble mean for central collisions is $\langle p_t \rangle_h \approx 0.5$ GeV/c, a factor 2.4 smaller than that for p-p collisions.

The evolution from peripheral HC on the left to central HC on the right proceeds most rapidly about a sharp transition near $\nu = 3$. The ratio of $\langle p_t \rangle_h$ for peripheral vs central (≈ 2.5) is the same as that at 2.76 TeV. In the same transition interval near $\nu = 3$ 200 GeV jet-related angular correlations change rapidly from a Glauber N-N linear superposition trend to substantial changes in certain jet properties [27]. We thus have strong evidence that the $\langle p_t \rangle_h(\nu)$ trend inferred from 2.76 TeV Pb-Pb collisions reflects parton fragmentation to jets evolving with A-A centrality according to pQCD principles in a manner very similar to that at 200 GeV, as in Fig. 8.

B.   N-N first encounters and hadron production

Reference [4] describes an oft-cited A-A hadron production model based on the assumption that of total p-p multiplicity n_{pp} a fraction x arises from "hard" processes and a fraction $1-x$ arises from "soft" processes, which is the TCM for p-p collisions. The result for A-A collisions satisfying the eikonal approximation and scaling with the corresponding Glauber parameters is then the expression

$$\frac{2}{N_{part}} n_{ch} \; = \; n_{pp}[1 + x(\nu - 1)] \qquad (12)$$

with $x = n_h/n_{pp}$ which describes hadron production for more-central Au-Au collisions well. However, the implicit assumption that x is the same for all cases is not correct. If $x \approx 0.1$ in more-central Au-Au as observed [16] it should have the same value for p-p collisions. But the observation is $x \approx 0.015$ for 200 GeV p-p collisions [1, 24].

To resolve the apparent inconsistency we can retreat to the more general expression

$$\frac{2}{N_{part}} n_{ch} \; = \; n_s + n_h(\nu)\nu \qquad (13)$$
$$= \; n_s[1 + x(\nu)\nu]$$

where $x(\nu) = n_h(\nu)/n_s$. Given the assumption that $n_h(\nu)$ is the same for all ν N-N encounters Eq. (13) does not describe hadron production data for more-central Au-Au collisions unless $x(\nu)$ has a complex structure. In order to arrive at Eq. (12) we must assume that in its first N-N encounter a nucleon contributes the p-p value $n_{h,pp}$ and in $\nu - 1$ subsequent encounters it contributes on average a different value $n_h(\nu)$. We then have $n_{pp} = n_s + n_{h,pp}$, $x(\nu) = n_h(\nu)/n_{pp}$ and all aspects are consistent with Eq. (12) that describes A-A data.

The success of Eq. (12) in describing hadron production data for which $x(\nu)$ varies simply from peripheral (N-N) to central A-A collisions implies that the first encounter of a projectile nucleon is special. An encounter with at least one unstruck (unexcited) nucleon produces jet-related hadrons as a p-p collision no matter what the A-B environment. In secondary encounters N-N collisions produce more jet-related hadrons, the extent depending on the A-B context. The first-encounter effect may reflect the extent to which colored partons are shielded within a hadron before and after it is excited.

C.   Comparing theory Monte Carlos with the TCM

In Fig. 3 of Ref. [17] several theory Monte Carlo models are compared with the $\langle p_t \rangle$ data, and in various ways the MCs fail. We argue that a common problem is the description of jets in high-energy nuclear collisions. In contrast, a simple jet description within the TCM based on pQCD principles and jet measurements provides an accurate and comprehensive description of the $\langle p_t \rangle$ data.

The PYTHIA MC includes jet production as a principal mechanism, but based on an eikonal model of colliding composite projectiles that is inconsistent with measured jet production in p-p collisions. Thus, in Fig. 3 (top panel) of Ref. [17] default PYTHIA [5] exhibits the characteristic $n_{ch}^{1/3}$ trend of the eikonal approximation (open diamonds). It is only by adding an ad hoc MPI color reconnection mechanism that the MC results can be made to accommodate the p-p $\langle p_t \rangle$ data. In contrast, a TCM with non-eikonal trend derived from p-p data describes the $\langle p_t \rangle$ data for a broad range of energies in Fig. 3 (left panel) of the present study to the uncertainty limits of the data. An unanticipated result of the TCM p-p analysis is the revelation that the energy dependence of $\langle p_t \rangle_h(\sqrt{s})$ is consistent with the energy dependence of minimum-bias jet spectrum widths [24], further buttressing a jet interpretation for the TCM hard component.

Some of the MC models for larger A-B systems are based on PYTHIA and thus inherit the problem of the eikonal approximation for N-N collisions. Although that approximation is valid for superposition of N-N collisions within A-A collisions the N-N collisions are not modeled correctly. An example is HIJING [2] based on PYTHIA which fails to describe Au-Au jet-related correlation data within a centrality interval where the data follow a Glauber linear superposition trend [27]. HIJING correctly implements the Glauber model of A-A collisions and could therefore be considered a representative example of the A-A TCM, but the PYTHIA modeling of jet production within HIJING N-N collisions is incorrect. The AMPT MC [6] is in turn based on HIJING but with the addition of final-state parton and hadron rescattering. AMPT inherits the PYTHIA problem within a more-complex parametrized system.

Monte Carlos in which hydrodynamic flow of a thermalized medium plays a dominant role [8] cannot describe jet manifestations in more-peripheral A-A collisions and therefore cannot provide a comprehensive description of A-A collisions. The basis for parametrization of hydro collision models can be questioned if such parametrizations are based on the data system to be described. In contrast, the TCM is required to describe all collision systems consistently with a minimal set of parameters whose values are determined transparently. The present analysis demonstrates that a TCM based on the universality of jets leads to comprehensive and accurate descriptions of a broad range of nuclear collision data and new insights into jet formation.

D.   What can be learned from the LHC $\langle p_t \rangle$ data?

Viewed within a TCM context the recent LHC $\langle p_t \rangle$ data are quite informative. A TCM based on simple jet contributions is found to describe $\langle p_t \rangle$ data accurately and consistently for a variety of collision systems. Alternative MC models strongly disagree with the data. Effective spectrum p_t cutoffs can be inferred accurately from $\langle p_t \rangle$ vs n_{ch} trends combined with the TCM spectrum soft-component model. The TCM soft component is universal, remains the same for all A-B combinations over a large energy interval. The non-eikonal nature of jet production in p-p collisions is confirmed by $\langle p_t \rangle$ data.

The p-p $\langle p_t \rangle$ hard component $\langle p_t \rangle_h(\sqrt{s})$ is observed to scale linearly with $\Delta y_{max} = \ln(\sqrt{s}/3 \text{ GeV})$ representing the widths of MB jet spectra from 200 GeV to 7 TeV [24]. The linear relation is just that expected if the TCM spectrum hard component represents jet fragments as described by pQCD [3]. That result is in turn consistent with the $\langle p_t \rangle$ hard component amplitude scaling as $n_h \propto (\Delta y_b)^2 = [\ln(\sqrt{s}/10 \text{ GeV})]^2$ implying non-eikonal jet production in p-p collisions [24].

The $n_h(\nu)$ and $\langle p_t \rangle_h(\nu)$ centrality trends in 2.76 TeV Pb-Pb are generally consistent with results from 200 GeV Au-Au collisions. Spectrum evolution in the latter system follows a pQCD description of FFs in which FF evolution tends to conserve the leading-parton energy but with a shift to lower-momentum fragments. A single QCD parameter describes the FF evolution in A-A.

From the variation with centrality of hadron production in 200 GeV Au-Au and 2.76 TeV Pb-Pb collisions we already see evidence for a difference between the first N-N encounter and subsequent N-N collisions. Applying the same approach to total hard $P_{t,h}$ production reveals a similar trend in 2.76 TeV Pb-Pb collisions. In peripheral A-A collisions the second N-N encounter produces more $P_{t,h}$, and thereafter the $P_{t,h}$ per N-N collision increases to a larger constant value. The ratio of peripheral to central A-A $\langle p_t \rangle_h$ values is similar (≈ 2.5) at the two energies.

Finally, in 5 TeV p-Pb collisions we observe a smooth transition from p-p non-eikonal to A-A eikonal jet-related trends with increasing n_{ch}, possibly a simple matter of competing probabilities for two production mechanisms

at a given total n_{ch}.

When combined with previous measurements of yields spectra and correlations in a TCM context the LHC $\langle p_t \rangle$ data provide strong evidence that in any collision system jet production is responsible for nearly all P_t and hadron production exceeding a universal soft component.

E. What role do flows play in p_t production?

It can be argued that hydrodynamic flows resulting from partonic and/or hadronic rescattering play a dominant role in A-A collisions at the RHIC and LHC based on many published results from spectrum and angular-correlation analysis. Radial flow has been inferred from analysis of single-particle spectra for identified hadrons, and popular convention assumes that increase of $\langle p_t \rangle$ with A-A centrality reflects increasing radial flow as noted in Ref. [17]. Elliptic flow appears to be described quantitatively by hydro theory including the mass splitting of $v_2(p_t)$ at low p_t. More recently, claimed observations of higher harmonic flows seem to complete the picture of a flow-dominated A-A collision scenario. One can then question an attempt to describe certain restricted aspects of collision data with a TCM including no flow component as in the present study.

This study considers the $\langle p_t \rangle$ systematics reported in Ref. [17] within a larger context established by a broad array of spectrum and correlation analyses as described for instance in Refs. [1,14-16,19,23-32]. Although $\langle p_t \rangle$ appears to be a simple quantity it can nevertheless provide stringent model tests as illustrated in Ref. [17] where all invoked MC models are falsified by the LHC $\langle p_t \rangle$ data. In contrast, the simple TCM with its hard (jet) component accurately describes all the LHC $\langle p_t \rangle$ data. No flow mechanism is *required* to describe those data.

It is widely assumed that flows dominate heavy ion collisions at the RHIC and LHC but there is actually substantial differential evidence to the contrary, as reviewed in Ref. [19]. Differential analysis of the centrality evolution of hadron p_t spectra indicates that there is no significant structure corresponding to radial flow (see Ref. [19]). In Ref. [16] the spectrum structure responsible for "radial flow" as inferred from so-called blast-wave model fits to single-particle identified-hadron spectra is shown to result from parton fragmentation to jets. The spectrum evolution with Au-Au centrality is described quantitatively and accurately by a pQCD calculation in Ref. [3] as described in Sec. VIII A. In blast-wave fits the question of accuracy (e.g., fit residuals) is not considered.

The systematics of jet-related 2D angular correlations in RHIC Au-Au collisions are reported in Ref. [27], and their quantitative correspondence with jet-related spectrum structure is established in Ref. [28]. The survival of intact minijets in central Au-Au collisions as established in Ref. [27] belies any significant partonic or hadronic rescattering that might drive transverse flows. $\langle p_t \rangle$ fluctuations conventionally expected to indicate temperature fluctuations near a QCD phase boundary are shown to be entirely due to minimum-bias jets in Refs. [14,15].

A significant cylindrical quadrupole component of 2D angular correlations is not related to jets, but the centrality and energy systematics of the nonjet quadrupole (what v_2 is intended to represent) are shown to contradict conventional hydro expectations in Ref. [30]. The quadrupole systematics do not relate to the strong jet modifications observed in more-central Au-Au collisions, as might be expected if formation of a dense bulk medium (QGP) were the common basis for both jet modification and hydro flows as noted in Ref. [19]. The production mechanism for the nonjet quadrupole is an open question, but recent pQCD theory predictions for p-p v_2 including a color-dipole approximation are promising [33].

As to flow harmonics, Ref. [34] is one example of several papers on that topic demonstrating that what has been promoted as "higher harmonic flows" actually represents the azimuth Fourier components of jet angular correlations described quantitatively by pQCD (see Sec. VIII F).

The present study demonstrates that a TCM including jet production as hard component and no flow contribution accurately describes $\langle p_t \rangle$ systematics for p-p, p-A and A-A collision systems and a broad range of collision energies whereas other models cannot do so. One of the most remarkable results appears in Fig. 4. The inferred hard component of the p-p $\langle p_t \rangle$ n_{ch} trend (left panel) varies with collision energy proportional to the width of the minimum-bias jet energy spectrum (right panel), just as expected if the hadron p_t spectrum hard component is a jet fragment distribution, as described in Refs. [3,16].

F. Can jets explain the "ridge" without flows?

It can be argued that the phenomenon described as the "ridge," referring to same-side (SS, $\phi \approx 0$) 2D correlation structures extended to large η values but narrow on ϕ, first observed at the RHIC and more recently with greater η extension at the LHC, cannot be explained by a jet mechanism because assumed jet structure (2D intrajet angular correlations) is narrow on η as well as ϕ. The "ridge" must then be a manifestation of collective expansion described by hydro, and flows must then be included in any description of high-energy nuclear collisions.

However, certain properties conventionally attributed to same-side 2D jet structure can be questioned. To simplify the argument it should be noted that the various "higher harmonics" v_m inferred from 1D Fourier analysis at large η difference (η_Δ or $\Delta\eta$) and subjected to hydro descriptions are mathematically equivalent to (sum to) a single narrow Gaussian on ϕ with azimuth width always identical to the acknowledged same-side 2D jet peak [34]. Debate must then focus on the relation (if any) of QCD jet production to that η-elongated "ridge" structure.

Dijets appearing in p-$\bar{p}$ or p-p collisions at RHIC energies (e.g. 200 GeV) are already very different from invacuum q-$\bar{q}$ dijets as observed at the LEP [3, 23]. Given

that jets are strongly modified ("quenched") in more-central A-A collisions we should compare *three* cases: e^+-e^- jets, p-p jets and A-A jets. What is the "standard" QCD dijet and what structural deviations are significant?

Color connection is an important aspect of in-vacuum jet structure, as demonstrated exhaustively by analysis of LEP three-jet events (q-$\bar{q}$-gluon) where the additional energetic gluon strongly distorts the default linear dipole field (string) that would appear in the q-$\bar{q}$ system in isolation and develop into an ideal symmetric LEP dijet.

In p-p collisions the situation is more complex, depending on the nature of the hard momentum transfer and the presence of the underlying event. In essence, the center of the string (color field) that should extend between two recoiling color charges is observed to be missing from p-p dijets (typically half the expected fragments) [3, 38]. It is possible that the struck partons evolving into a p-p dijet are not themselves color connected as a pair. They may share a common momentum transfer but not a color field. Instead, each struck parton remains connected to the color hole it left in the parent projectile nucleon. That possibility could correspond to dijet production by exchange of a color-singlet hard Pomeron. The more energetic the struck parton the larger the x value (and hence lab rapidity) of the hole, thus the longer the hadron fragment "ridge" that emerges from the sideways color field.

Such a QCD jet mechanism could explain the ridge phenomenon and its systematics. By selecting minimum-bias jets (minijets, $x \approx 0.03$) the jet-related "ridge" in RHIC central Au-Au may be so short that it appears only as η elongation of the SS 2D peak still well-described on η by a single Gaussian, as first reported by STAR in 2004 [35]. If p_t cuts are applied to force more-energetic leading partons (from larger $x \approx 0.1$) the corresponding non-Gaussian "ridge" may be extended to larger rapidities [36]. Such a QCD-jet "ridge" mechanism should be *expected* based on known jet physics. At LHC energies the x range is substantially larger than at RHIC and the MB jet spectrum is much broader, so one should expect longer "ridge" extensions at the higher energies as observed. There is thus no reason at present to exclude a QCD jet explanation for SS η-extended structures.

IX. SUMMARY

Recent measurements of event-ensemble mean transverse momentum $\langle p_t \rangle$ vs charged-hadron multiplicity n_{ch} for p_t spectra from 5 TeV p-Pb and 2.76 TeV Pb-Pb collisions and from p-p collisions for several energies were compared to several theory Monte Carlos. In most cases there are severe disagreements between theory and data, leaving interpretation of the $\langle p_t \rangle$ data unresolved.

In the present study we develop a two-component model (TCM) for total P_t production (within some angular acceptance) in high energy nuclear collisions based on previous measurements of dijet production, parton fragmentation and jet spectra. The underlying assumption of the TCM is that of two contributions to $P_t = P_{t,s} + P_{t,h}$ the soft component is a universal feature of high energy collisions corresponding to longitudinal dissociation of participant nucleons. The complementary hard component is entirely due to minimum-bias jet production in N-N collisions. The same model is applied to charged-hadron production in the form $n_{ch} = n_s + n_h$.

Given TCMs for P_t and n_{ch} we obtain the TCM for $\langle p_t \rangle$ as P_t/n_{ch}. A key feature of the $\langle p_t \rangle$ TCM is the observation that jet production in p-p collisions does not follow a semiclassical eikonal approximation as commonly assumed in p-p Monte Carlo models. The observed non-eikonal production trend is incorporated into the TCM for this study. Models for p-p and A-A collisions are derived separately depending on the relation to the eikonal approximation and applicability of the Glauber model to A-A collisions. To aid data comparison we develop a correction for biases due to incomplete p_t acceptance.

Aside from confirming the non-eikonal nature of p-p jet production the main result of the p-p TCM analysis is extraction of a $\langle p_t \rangle$ hard component $\langle p_t \rangle_h(\sqrt{s})$ for several collision energies. The energy variation of the hard component is found to be linearly related to parameter $\Delta y_{max} = \ln(\sqrt{s}/3 \text{ GeV})$ which, in a separate study of jet systematics, is observed to describe the energy dependence of minimum-bias jet spectrum widths. The linear relation is understandable in a context where $\langle p_t \rangle_h$ is determined by a hadron spectrum hard component composed of jet fragments described by folding a fragmentation-function ensemble with a minimum-bias jet spectrum. The jet interpretation is strongly supported.

The Pb-Pb $\langle p_t \rangle$ analysis has several implications. The $P_{t,h}$ production generally follows binary-collision scaling according to the eikonal approximation as expected for jet production in A-A collisions. However, as for hadron production the data suggest that the first N-N encounter of a nucleon participant in an A-A collision is special, yielding the same results as a p-p collision. Subsequent encounters produce different results (more hadron fragments per N-N encounter, reduced $\langle p_t \rangle_h$) with increasing A-A centrality. The increase of n_h and decrease of $\langle p_t \rangle_h$ is consistent with modifications to jet fragment distributions (hard components) observed in hadron p_t spectra. The systematics of jet modification in 2.76 TeV Pb-Pb collisions appears to be very similar to those in 200 GeV Au-Au collisions, the only differences being (a) the location of a sharp transition from N-N linear superposition (A-A transparency) to strongly modified jets and (b) increase of soft multiplicity and hard jet-related components by factors $\ln(\sqrt{s_{NN}}/10 \text{ GeV})$ and $\ln^2(\sqrt{s_{NN}}/10 \text{ GeV})$ respectively as extrapolated from spectrum and correlation systematics at RHIC energies.

Generally speaking the TCM for $\langle p_t \rangle$ data provides a very compact data representation. Much of the model is determined by prior measurements of other aspects of high energy nuclear collisions. The novelty arising in the $\langle p_t \rangle$ study is (a) the energy dependence of $\langle p_t \rangle_h(\sqrt{s})$

for p-p collisions found to comply with previously measured jet spectrum systematics, (b) the participant first-encounter effect already implicit in hadron production systematics and (c) variation of $\langle p_t \rangle_h(\nu)$ with Pb-Pb centrality which is qualitatively consistent with jet modifications in 200 GeV Au-Au collisions described by pQCD.

The p-Pb results, which are said to present conceptual difficulties, appear to be consistent with the TCMs for p-p and A-A collisions, transitioning smoothly from the p-p trend at lower multiplicities (quantitative agreement) to a Glauber-linear-superposition model of A-A collisions with no modification of jet fragmentation in more-central collisions (close agreement with the functional form).

To conclude, this study presents a TCM that can describe all $\langle p_t \rangle$ vs n_{ch} data from the LHC within their uncertainties. The TCM is a *sufficient* (and very simple) model for those data. One can therefore logically conclude that hydro-based and other complex Monte Carlo models applied to the same data are not logically *necessary*. The TCM description implies that variation of $\langle p_t \rangle$ at the LHC is caused by variation of dijet production.

This material is based upon work supported by the U.S. Department of Energy Office of Science, Office of Nuclear Physics under Award Number DE-FG02-97ER41020.

Appendix A: Two-component Model

The two-component model (TCM) of hadron production in high energy nuclear collisions refers variously to a phenomenological description of the n_{ch} dependence of p_t spectra from 200 GeV p-p collisions [1], to an *a priori* expectation for mid-rapidity hadron production at the RHIC [4] and to a subsequent overarching TCM for yields, spectra and two-particle correlations with direct connections to pQCD predictions of dijet fragment yields [3, 16, 28]. In this Appendix I review aspects of the TCM relevant to its application in the present study.

1. TCM description of p-p p_t or y_t spectra

Systematic analysis of the n_{ch} dependence of p_t spectrum shapes from 200 GeV p-p collisions described in Ref. 1 led to a compact phenomenological TCM with *factorization* of multiplicity and rapidity dependence in the form [1]

$$\frac{d^2 n_{ch}}{y_t dy_t d\eta} = S(y_t, n_{ch}) + H(y_t, n_{ch}) \quad (A1)$$
$$= \rho_s(n_{ch})S_0(y_t) + \rho_h(n_{ch})H_0(y_t)$$

with $\rho_x = n_x/\Delta\eta$. Unit-integral soft-component model S_0 is consistent with a Lévy distribution on m_t defined by Eq. (5). Hard-component model H_0 is approximated by a Gaussian on y_t centered at $y_t \approx 2.65$ ($p_t \approx 1$ GeV/c). Those assignments do not rely on an *a priori* physical

model. Integration of Eq. (A1) over y_t and some angular acceptance $\Delta\eta$ results in $n_{ch} = n_s + n_h$. Spectrum data presented in Fig. 1 indicate that $\rho_h = \alpha\rho_s^2$ with $\alpha \approx 0.006$. The combination is a quadratic equation that uniquely defines n_s and n_h in terms of n_{ch}.

Figure 1 (left panel, $\Delta\eta = 1$) demonstrates that decomposition of y_t spectra as in Eq. (A1) leads to factorization of $H(y_t, n_{ch}) = n_h(n_{ch})H_0(y_t)$ to good approximation. The resulting values of $n_h(n_{ch})$ in the right panel follow the trend $n_h \propto n_s^2$ also to good approximation. In Ref. [1] the inferred trend $n_h/n_{ch} \propto n_{ch}$ seemed to indicate saturation for larger n_{ch}. It was later realized that n_s is the preferred control parameter for the p-p TCM.

The Lévy distribution defined by Eq. (5) is similar in form to the "power-law" model function that has been used to fit p_t or m_t spectra [12]. However, a single Lévy function alone cannot describe p-p spectra accurately, as demonstrated in Ref. [1]. The two-component spectrum model of Eq. (A1) is *necessary* to describe an ensemble of y_t spectra representing a substantial multiplicity interval.

Physical interpretation of phenomenological TCM elements has proceeded by several routes: (a) correspondence with minimum-bias two-particle correlations on $y_t \times y_t$ and $(\eta_\Delta, \phi_\Delta)$; (b) correspondence with pQCD predictions and (c) correspondence with other experimental results. In all cases soft and hard hadron production mechanisms are assumed to be linearly independent

2. Correspondence with two-particle correlations

Correlations on $y_t \times y_t$ are especially simple: a 2D peak below $y_t = 2$ ($p_t \approx 0.5$ GeV/c) interpreted as the soft component and a 2D peak above $y_t = 2$ interpreted as the hard component [37]. Angular correlations corresponding to the two $y_t \times y_t$ peaks are simply interpreted and confirm those assignments [26]. The $y_t \times y_t$ soft component is consistent with longitudinal fragmentation (single 1D Gaussian on η_Δ). The $y_t \times y_t$ hard component is consistent with MB dijets [2D same-side peak on $(\eta_\Delta, \phi_\Delta)$ representing single jets and 1D away-side peak on ϕ_Δ representing back-to-back jet pairs]. The 1D projection of the $y_t \times y_t$ 2D hard component is in turn consistent with 1D spectrum hard component $H(y_t)$. Generally, the two correlation components (including charge correlations) appear to represent two orthogonal fragmentation systems, each locally conserving net charge.

3. Correspondence with pQCD predictions

The hard-component shape $H(y_t, n_{ch})$ inferred from p-p spectra can be predicted quantitatively as a hadron fragment distribution [3] by convoluting a measured MB jet spectrum [38] with measured fragmentation functions (FFs) [39], both from 200 GeV p-$\bar{p}$ collisions. The quantitative agreement confirms a jet mechanism for the p-p TCM spectrum and correlation hard components.

There are four possibilities for the FF choice in the pQCD convolution: quark or gluon FFs inferred from e^+-e^- or p-$\bar{p}$ collisions. It is notable that e^+-e^- and p-$\bar{p}$ FFs are quite different for smaller fragment momenta, but further discussion is outside the scope of this study. As to quark or gluon FFs the two are quite different for larger parton energies due to the different color charges, however for smaller parton energies the two FF systems converge [23]. The spectrum hard component from 200 GeV p-p collisions favors quark-jet FFs from p-$\bar{p}$ collisions [3]. That result is reasonable at RHIC energies since larger hadron fragment momenta correspond to larger momentum fraction x and therefore valence quarks. Smaller fragment momenta correspond to low-energy jets for which quark and gluon FFs are equivalent.

4. Correspondence with other experimental results

The dijet production trend $n_h \propto n_s^2$ inferred from p-p hadron spectra as described above combined with $dn_s/d\eta \propto \ln(\sqrt{s}/10 \text{ GeV})$ has been used to describe jet-spectrum energy trends quantitatively over large p-p collision-energy and jet-energy intervals [38]. The predicted jet spectrum trends can then be combined with

measured FFs to calculate spectrum hard component $H(y_t)$ [3]. TCM results inferred from p-p collisions can be used to predict hadron production [28] and correlation [27] trends in A-A collisions over an extended centrality interval corresponding to linear superposition of N-N collisions. The expression $dn_s/d\eta \propto \ln(\sqrt{s}/10 \text{ GeV})$ above is based on interpreting the spectrum soft component as a manifestation of small-x gluons from dissociated projectile nucleons, the energy intercept 10 GeV inferred from jet-related correlation systematics [27].

The TCM for $\langle p_t \rangle$ vs n_{ch} defined in Sec. IV is based on a few simple assumptions consistent with the above: (a) A spectrum soft component with fixed Lévy form scales with n_{ch} in p-p collisions $\propto n_s$ and with centrality in A-A collisions $\propto N_{part}$, with form independent of collision multiplicity or energy. (b) A spectrum hard component scales with n_{ch} in p-p collisions $\propto n_s^2$ and with centrality in A-A collisions $\propto N_{bin}$, with form independent of n_{ch} in p-p collisions but varying with centrality in A-A collisions consistent with independent RHIC measurements and with QCD FFs modified in a single aspect: the coefficient of a gluon splitting function is increased leading to redistribution of leading-parton energy to smaller hadron fragment momenta [3] as described in Sec. VIII A.

[1] J. Adams *et al.* (STAR Collaboration), Phys. Rev. D **74**, 032006 (2006).
[2] X.-N. Wang, Phys. Rev. D **46**, R1900 (1992); X.-N. Wang and M. Gyulassy, Phys. Rev. D **44**, 3501 (1991).
[3] T. A. Trainor, Phys. Rev. C **80**, 044901 (2009).
[4] D. Kharzeev and M. Nardi, Phys. Lett. B **507**, 121 (2001).
[5] T. Sjöstrand, S. Mrenna and P. Z. Skands, Comput. Phys. Commun. **178**, 852 (2008); T. Sjöstrand and M. van Zijl, Phys. Rev. D **36**, 2019 (1987); T. Sjöstrand, Comput. Phys. Commun. **82**, 74 (1994);
[6] Z.-W. Lin, C. M. Ko, B.-A. Li, B. Zhang and S. Pal, Phys. Rev. C **72**, 064901 (2005).
[7] P. Huovinen and P. V. Ruuskanen, Ann. Rev. Nucl. Part. Sci. **56**, 163 (2006).
[8] T. Pierog, I. Karpenko, J. M. Katzy, E. Yatsenko and K. Werner, arXiv:1306.0121; K. Werner, Nucl. Phys. Proc. Suppl. **175-176**, 81 (2008).
[9] E. Schnedermann, J. Sollfrank, and U. Heinz, Phys. Rev. C **48**, 2462 (1993).
[10] L. McLerran, M. Praszalowicz and B. Schenke, Nucl. Phys. A **916**, 210 (2013).
[11] S. Gavin, L. McLerran and G. Moschelli, Phys. Rev. C **79**, 051902 (2009).
[12] C. Albajar *et al.* (UA1 Collaboration), Nucl. Phys. B **335**, 261 (1990).
[13] J. Adams *et al.* (STAR Collaboration), Phys. Rev. C **71**, 064906 (2005).
[14] J. Adams *et al.* (STAR Collaboration), J. Phys. G **32**, L37 (2006).
[15] J. Adams *et al.* (STAR Collaboration), J. Phys. G **33**, 451 (2007).

[16] T. A. Trainor, Int. J. Mod. Phys. E **17**, 1499 (2008).
[17] B. B. Abelev *et al.* (ALICE Collaboration), Phys. Lett. B **727**, 371 (2013).
[18] B. I. Abelev *et al.* (STAR Collaboration), Phys. Rev. C **79**, 034909 (2009).
[19] T. A. Trainor, J. Phys. G **37**, 085004 (2010).
[20] K. Aamodt *et al.* (ALICE Collaboration), Phys. Rev. Lett. **106**, 032301 (2011).
[21] V. Khachatryan *et al.* (CMS Collaboration), JHEP **1009**, 091 (2010).
[22] B. Abelev *et al.* (ALICE Collaboration), Phys. Lett. B **719**, 29 (2013).
[23] T. A. Trainor and D. T. Kettler, Phys. Rev. D **74**, 034012 (2006).
[24] T. A. Trainor, Phys. Rev. D **89**, 094011 (2014).
[25] T. A. Trainor, Phys. Rev. D **87**, 054005 (2013).
[26] R. J. Porter and T. A. Trainor (STAR Collaboration), J. Phys. Conf. Ser. **27**, 98 (2005).
[27] G. Agakishiev, *et al.* (STAR Collaboration), Phys. Rev. C **86**, 064902 (2012).
[28] T. A. Trainor and D. T. Kettler, Phys. Rev. C **83**, 034903 (2011).
[29] R. J. Porter and T. A. Trainor (STAR Collaboration), PoS **CFRNC2006**, 004 (2006).
[30] D. T. Kettler (STAR collaboration), Eur. Phys. J. C **62**, 175 (2009).
[31] T. A. Trainor, arXiv:1402.4071.
[32] T. A. Trainor and D. J. Prindle, hep-ph/0411217.
[33] B. Z. Kopeliovich, A. H. Rezaeian and I. Schmidt, Phys. Rev. D **78**, 114009 (2008).
[34] T. A. Trainor, J. Phys. G **40**, 055104 (2013).
[35] J. Adams *et al.* (STAR Collaboration), Phys. Rev. C **73**,

064907 (2006).

[36] B. I. Abelev *et al.* (STAR Collaboration), Phys. Rev. C **80**, 064912 (2009).

[37] E. W. Oldag (STAR Collaboration), J. Phys. Conf. Ser. **446**, 012023 (2013).

[38] T. A. Trainor, Phys. Rev. D **89**, 094011 (2014).

[39] D. Acosta *et al.* (CDF Collaboration), Phys. Rev. D **68**, 012003 (2003).